Ultrasonics Sonochemistry 73 (2021) 105475

Contents lists available at ScienceDirect

Ultrasonics Sonochemistry

journal homepage: www.elsevier.com/locate/ultson

Ultrasonic-assisted electrodeposition of Ni/diamond composite coatings and its structure and electrochemical properties

Baosong Li [a,*], Tianyong Mei [a], Hongqiang Chu [a], Jiajia Wang [a], Shengsong Du [a], Yicheng Miao [a], Weiwei Zhang [b,*]

[a] College of Mechanics and Materials, Hohai University, Nanjing 211100, China
[b] College of Mechanical and Electrical Engineering, Hohai University, Changzhou 213022, China

ARTICLE INFO

Keywords:
Ni/diamond composite coating
Electrodeposition
Electrochemical impedance spectroscopy
Ultrasonic-assisted
Magnetic stirring

ABSTRACT

Ni/diamond composite coatings have been synthesized by ultrasonic-assisted electrodeposition in a Ni electroplating bath containing diamond nanoparticles. The influences of current density and ultrasonic agitation on the coating composition, morphology, topography, phase structure, and electrochemical characteristics of the electrodeposits were evaluated. Ultrasonic agitation was provided using an external ultrasonic bath at a frequency of 40 kHz and acoustic power of 300 W. Coating samples were also prepared under magnetic stirring for comparison with the ultrasonic-assisted deposits. This work reveals that the diamonds have been incorporated and evenly distributed in the composites. The coatings exhibit dense, granular like morphology with pyramid-like grains. As current density increases, the diamond amount of ultrasonic-assisted electrodeposits first increased to maximum of 11.4 wt% at 3 A dm^{-2} and then decreases to 9.9 wt% at 5 A dm^{-2}, and the RTC of the preferred orientation (200) plane increases from 76.3% up to 93.4%. The crystallite size was 60–80 nm and the R_a of the magnetic and ultrasonic agitations were 116 nm, 110 nm, respectively. The maximum R_p of 39.9, 50.3 kΩ cm^2 was obtained at 4 A dm^{-2} when respectively immersed 30 min and 7 days, illustrating the best corrosion resistance of the coatings of 4 A dm^{-2}. The effects of mechanical and ultrasonic agitations on the mechanism of the co-electrodeposition process were both proposed. The incorporation of diamond particles enhances the hardness and wear-resisting property of the electrodeposits. The ultrasonic-assisted electrodeposited Ni/diamond coating has better corrosion resistance than that prepared under mechanical stirring conditions.

1. Introduction

Among many metallic matrices, nickel was widely used as protective material due to its desirable characteristics, including excellent ductility, corrosion resistance, and chemical stability [1,2]. It can be applied in many industries like automotive parts, oil and gas instruments, decorative materials and protective coating. However, the mechanical strength and wear resistance of pure nickel are not high enough to meet the requirements of the application in some harsh fields, for example, marine environment, which restricts its application [3,4]. To enhance the properties of nickel, one method was to develop Ni-based alloys [5], such as Ni-Co alloys. Aliofkhazraei et al. [6] reviewed the electrodeposited Ni-Co alloy and introduced the mechanism of electrodeposition and effect of process parameters on the microstructure, mechanical, electrochemical and tribological characteristics. The other method was to co-electrodeposition reinforcing particles in the nickel or its alloy matrix to improve its properties such as abrasion resistance, hardness and corrosion stability.

Recently, researchers indicated that the addition of SiC [7,8], ZrO_2 [9], TiN [10], Al_2O_3 [11], and diamond [12,13] reinforcing particles into the Ni matrix can improve its hardness, wear and corrosion resistance. Among these strengthening candidates, diamond has been often investigated and employed to prepare wear-resistant coatings, due to its outstanding hardness, wear resistance and chemical inertness [12,14]. Deng et al. [15] produced Ni/diamond films as dicing blades to improve their properties and found that adding 0.1–0.2 g L^{-1} BEO enhanced the hardness and wear resistance with high diamond content embedded in the coating. Sajjadnejad et al. [16] prepared Ni/diamond coatings by pulse electroplating from an additive-free Watts bath and illustrated that incorporation of the diamond particles increased the corrosion-resistant capability. Zhou et al. [13] reported that the presence of Co^{2+} can improve the particle content in the composite electrodeposits. Bao et al.

* Corresponding authors.
E-mail addresses: lbs79@126.com (B. Li), zdzdq@126.com (W. Zhang).

https://doi.org/10.1016/j.ultsonch.2021.105475
Received 11 December 2020; Received in revised form 6 January 2021; Accepted 20 January 2021
Available online 2 February 2021

[17] have investigated the mechanical properties of Ni/diamond coatings by traditional, sediment and burying electro-codeposition methods. Huang et al. [18] studied the high-particle-content Ni/diamond coating and proved that the particle content was effectively enhanced employing two-step electrophoretic and electrodeposition means, resulting in an effective improvement in wear resistance. Makarova et al. [19] electrodeposited nickel-nanodiamond coatings from tartrate electrolyte and reported that the addition of 5 g L^{-1} nanodiamonds could strengthen the microhardness, wear resistance, and corrosion resistance. Almost all scholars believe that the diamond incorporations can perfect the abrasion and corrosion performance of the Ni coatings [20].

Besides, nanoparticles are easily agglomerated, which could lead to uneven distribution and low performance of the composite coatings [21]. Now, it remains a long-term challenge to uniformly disperse the particles in the matrix. Therefore, ultrasonic-assisted techniques were developed. Ma et al. [22] investigated Ni-Al_2O_3 coatings with the assistance of ultrasound and illustrated that a suitable ultrasonic power benefits the co-deposition and uniform dispersion of Al_2O_3 particles in nickel coating. Cui et al. [23] reported that Ni/TiN composite coating electrodeposited at ultrasonic intensity 20 W/cm^2 has compact morphology, high TiN nanoparticles content in composite coating and improved anti-corrosion properties. Tudela et al. [24] introduced that ultrasonic agitation could change the preferred orientation and benefit fine grains. Ultrasonic-assisted electrodeposition facilitates the uniform distribution of particles in solution and metallic matrix composites [25]. Besides, ultrasound can promote mass transport, reduce the diffuse layer thickness [26,27] and increase the growth rate of the Ni/diamond composite coatings.

Although some articles have already reported the electrodeposited Ni/diamond composite coatings[28,29], few efforts have been concerned on the effects of agitation modes and current density on the fabrication and characterization of Ni/diamond composite coatings by direct current deposition. To the knowledge of us, few results are available for the ultrasonic-assisted electrodeposition of Ni/diamond composite coating. Therefore, in the current study, Ni/diamond composite coatings were synthesized by ultrasonic-assisted electrodeposition. The effect of current density and agitation mode (mechanical and ultrasonic agitations) on the surface morphology, phase structure, surface topography, composition and related mechanism of the electrodeposits were comparatively investigated. The electrochemical properties of Ni/diamond composite coatings were also investigated. The motivation of adopting ultrasonic assistance was to improve the uniform distribution of diamond particles as well as inhibit its agglomeration in the metallic matrix, then enhance the quality of the composites.

2. Experimental

2.1. Synthesis of Ni/diamond composite coatings

Commercially available diamond particles (Henan Yalong Superhard Materials Co., Ltd.) were used in this studied. The Ni/diamond composites have been coated on brass sheets in an electroplating bath. For comparison, the samples were also electrodeposited under magnetic stirring. Nickel was acted as the anode and brass was used as the cathode. The constituents of the electroplating bath and process parameters are summarized in Table 1. In this plating bath, $NiSO_4{\cdot}6H_2O$, $NiCl_2{\cdot}6H_2O$ supply Ni^{2+} ions. Chloride ions are beneficial to the conductivity of the electrolyte. Current density of 2, 3, 4, 5 A dm^{-2} in direct current mode were applied for the ultrasonic-assisted electrodeposition. The diamond nanoparticles were first adequately dispersed in a small amount of solution, then subjected to ultrasonic treatment. Then the treated concentrated diamond solution was poured into the bulk of the electrolyte. All reagents were analytical grade in purity. Fig. 1 describes the electrodeposition setup used in this work.

The brass substrate should be pretreated by polishing and rinsing for a smooth and clean surface. Then it was degreased by alkaline solution and ultrasonically treated in alcohol. Just before electrodeposition, the substrate was dipped in dilute HCl solution for no more than one minute to activate the surface. The electrodeposition time was adjusted based on current density to obtain the same thickness of the coatings. The Ni/diamond coatings have been electrodeposited under magnetic stirring at 400 rpm and ultrasonic dispersion at 300 W acoustic power and 40 kHz, respectively. Insulation was required for the non-working area of the substrate by polymer tape. Fig. 2. displays the electrodeposition process of the Ni/diamond coating. After electroplating, the obtained samples should be ultrasonically washed with deionized water to remove the attached diamonds, then naturally dried.

Table 1
Electroplating bath and process parameters of Ni/diamond composite coating.

Bath composition		Operating parameters	
$NiSO_4{\cdot}6H_2O$	280 g L^{-1}	Temperature	55 ± 2 ℃
$NiCl_2{\cdot}6H_2O$	40 g L^{-1}	Current density	2–5 A dm^{-2}
H_3BO_3	30 g L^{-1}	pH	4.2 ± 0.1
Sodium dodecyl sulfate (SDS)	0.001 g L^{-1}	Agitation	mechanical// ultrasonic
Diamond NPs	6 g L^{-1}	Deposition time	20–45 min

2.2. Characterization

The coatings were evaluated in terms of the morphology and chemical composition by FEI Inspect F50 SEM with EDS. The diamond particles were characterized by JEM-2000EX TEM. The surface topography and roughness were characterized by Bruker Dimension Icon AFM. ESCALAB 250X XPS spectrometer was utilized to analyze the surface features. SmartLab XE XRD operated at Cu-Kα radiation (λ = 1.5406Å) at a rating of 40 kV and 40 mA was utilized to examine the phase structure of the deposits. The scan rate was 10° min^{-1}. Debye-Scherer's equation was used to calculate the crystallite size of the electrodeposited Ni/diamond coatings.

$$D = \frac{K\lambda}{\beta\cos\theta}\ \frac{180}{\pi} \quad (1)$$

Where D represents the crystallite size, K is 0.9, λ is the X-ray wavelength (0.15406 nm). β refers to the full width at half maxima (FWMH) at the Bragg angle θ. The following Eq. (2) presents the relative texture coefficient (RTC) of Ni/diamond composite coating.

$$RTC(hkl) = \frac{Is(hkl)/\ I0(hkl)}{\sum {}_1^n Is(hkl)/\ I0(hkl)} \quad (2)$$

Where the I_s(hkl) and I_0(hkl) denote the peak intensity of Ni/diamond coating and the standard Ni powder (JCPDS No. 87–0712). XPS technique was used to analyze the chemical composition and the element chemical valence state. The electrochemical properties were tested with CHI660E potentiostat in a three-electrode cell in 3.5 wt% NaCl solution at normal temperature. Saturated calomel electrode (SCE), Pt and specimen with working area 1 cm^2 were acted as the reference, counter and working electrode, respectively. EIS was tested at E_{ocp} from 0.01 Hz to 100 kHz, with a disturbing amplitude of 10 mV after soaked 0.5 and 168 h. Tafel curves were conducted to analyze the corrosion resistance of the coatings.

3. Results and discussion

3.1. Characterization of the diamond particles

Fig. 3 displays the XRD spectrum and TEM image of the diamond particles. The highest diffraction peak that appeared at 43.86° was attributed to the (111) plane of the diamond. The peaks at 75.24° correspond to the (220) crystallographic plane. The results indicated

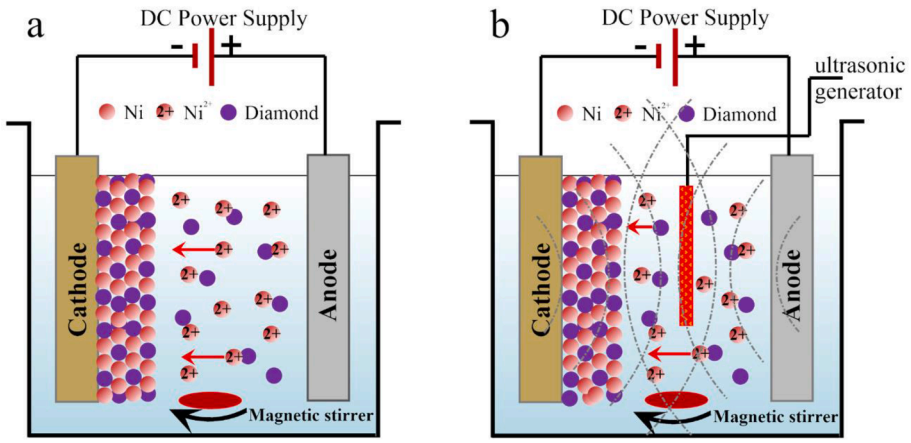

Fig.1. Schematic of the electrodeposition device for Ni/diamond composite coating assisted by (a) magnetic stirring, (b) ultrasonic agitation plus mechanical stirring.

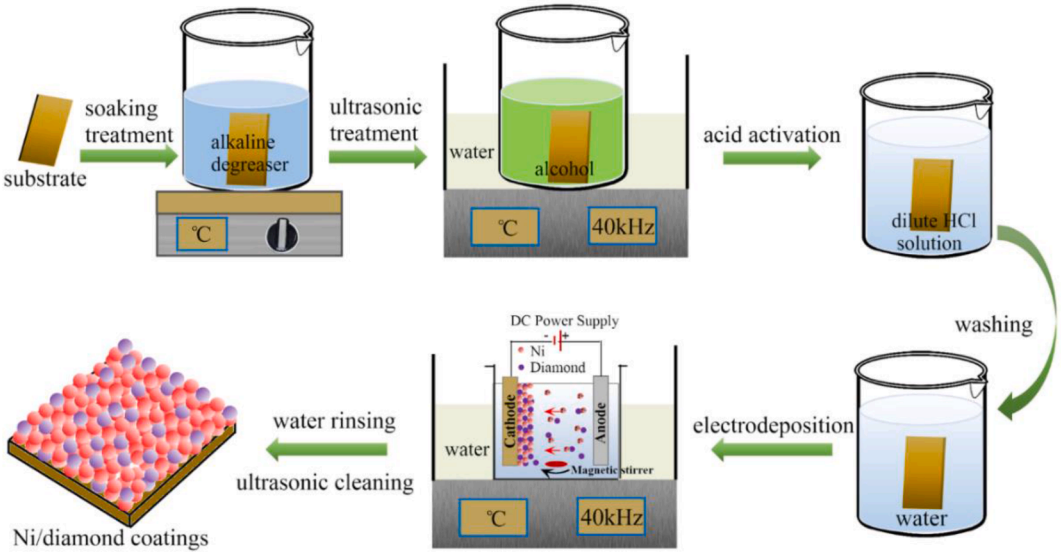

Fig. 2. Electrodeposition process of the Ni/diamond composite coating.

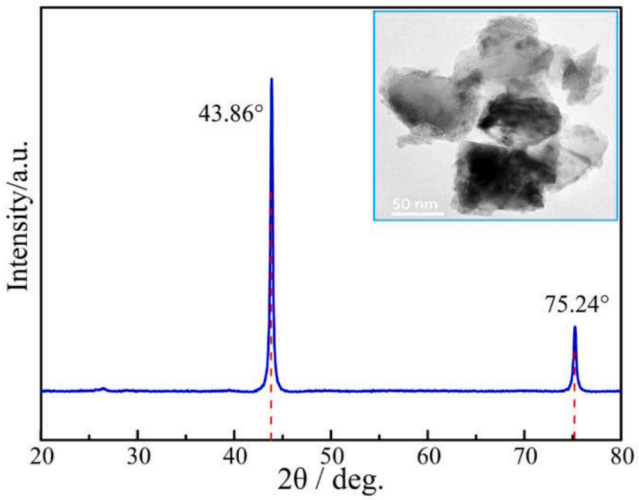

Fig. 3. XRD pattern and TEM images of the diamond particles.

that these diamond particles were crystal structure. The inlaid TEM image presents that the mean dimension of the diamond was about 60 nm. It was observed that the particles have irregular shapes with sharp edges, which were disadvantageous for the particle incorporation and uniform distribution in the nickel matrix.

3.2. *Surface morphology and coating composition*

Fig. 4 exhibits the optical photographs of Ni/diamond coating samples prepared at 4 A dm^{-2} under different agitation modes. The grey sample was roughly 20 mm × 20 mm in dimension. It shows that the substrate surface was homogeneously covered by the electrodeposits, and no cracks or pinholes were noticed in all the coatings. The particles were homogeneously dispersed in the coating. Compared to samples of magnetic stirring, the ultrasonic-assisted electrodeposited coatings have some protrusion structures. Noting that the distinct difference in surface morphology related to the stirring method. The coating deposited by the magnetic stirring method shows a smooth and grey surface. The Ni/diamond coating of magnetic stirring is similar to the pure Nickel coatings, which is better than ultrasonic stirring in terms of flatness, uniformity and glossiness. However, the surface of the Ni/diamond coating obtained with ultrasonic agitation has some protrusion structures.

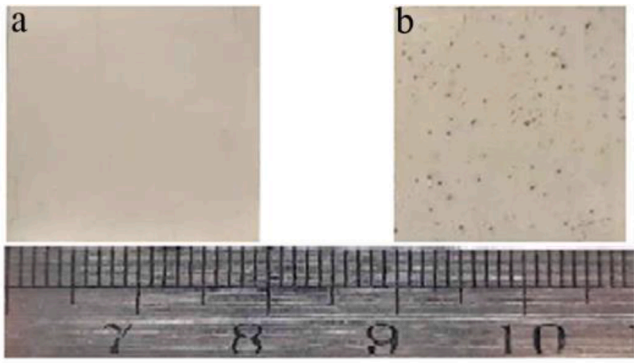

Fig. 4. Optical images of Ni/diamond coating prepared under (a) magnetic stirring; (b) ultrasonic agitation.

Fig. 5 presents the morphologies of the Ni/diamond coatings produced under magnetic stirring and ultrasonic agitation. All coatings are compact and show pyramids-like morphology, which is consistent with the traditional nickel coating. As shown in Fig. 5(a-c), the coatings produced under magnetic stirring have some adsorbed debris on the surface. Fine aggregates are gathered near the edges of the grains, which can be ascribed to the diamond particles. Unlike nodular shapes of the grains of the Ni–W [30,31], Ni-Co [32,33] matrix, the Ni/diamond shows pyramids-like grains. It indicated that more diamond particles aggregated when the coatings were deposited with magnetic stirring. Fig. 5(d-f) shows the morphologies of the coatings prepared by ultrasonic-assisted electrodeposition. Compared to magnetic stirring mode, the size of the crystal granules was relatively larger for ultrasonic-assisted electrodeposited coatings. It was noticed that the surface of the coating prepared by ultrasonic-assisted electrodeposition has large protrusions, which corresponds to the nanoparticle clusters caused during the co-deposition process. The reason might be that the growth rate of nickel crystals under ultrasonic mode was higher than that of mechanical ones. The amounts of aggregated particle clusters have been largely reduced by ultrasonic conditions. So, ultrasonic agitation benefits more on the particle co-deposition and uniform dispersion in the composites in comparison with the mechanical stirring mode. Moreover, ultrasonic waves can also accelerate the electrodeposition rate, resulting in the fast growth in grain size. Finally, the particle amounts and their dispersion in the composites were enhanced for ultrasonic-assisted electrodeposition.

Fig. 6 reveals the morphologies of Ni/diamond coatings prepared under ultrasonic and mechanical agitations at different current density. These coatings show compact and fine structure. First, it was evident that with the increase of the current density, the granule size of the coatings increased. It implied that the roughness of the deposits increased as the electroplating current density increased. The ultrasonic-assisted coatings have been compared with those prepared under magnetic stirring condition by careful observation. It demonstrated that the ultrasonic-assisted electrodeposited coatings (Fig. 6e-h) had fewer particle clusters in comparison with the coatings prepared at mechanical stirring conditions (Fig. 6a-d). The dispersion effect of mechanical agitation was lower than the ultrasonic treatment. So, mechanical stirring can't fully disperse the particle clusters, leading to uneven distribution in the composite. In contrast, the ultrasonic-assisted method is more beneficial to the particle uniform dispersion in the bath and nickel matrix.

The inlaid figure in Fig. 6 was the enlarged morphologies of these coatings. All coatings are dense, uniform, with pyramids-like morphology. From the enlarged images, it was found that the number of aggregated diamond particle clusters was greatly decreased under ultrasonic conditions. The dispersion of nanodiamonds in the Ni matrix has been improved by adopting ultrasonic-assisted electrodeposition.

Fig. 7 displays the element distribution maps of the coatings electrodeposited at 4 A dm^{-2} under magnetic and ultrasonic agitation, respectively. As seen in Fig. 7(a), several diamond aggregates were observed for the magnetic stirring electrodeposited coatings. As a contrast in Fig. 7(b), the ultrasonic-assisted electrodeposited Ni/diamond composite coating exhibits a uniform surface and no obvious aggregates were noticed. It indicated that the nanodiamonds were incorporated in the coating and the particle distribution in the matrix was uniform. As well known, the amounts and distribution of embedded nanodiamonds significantly affect the performance. The results suggested that nanodiamonds were strongly and evenly dispersed in ultrasonic-assisted electrodeposits. Table 2 reveals the chemical composition of Ni/diamond deposits. It indicated that the samples

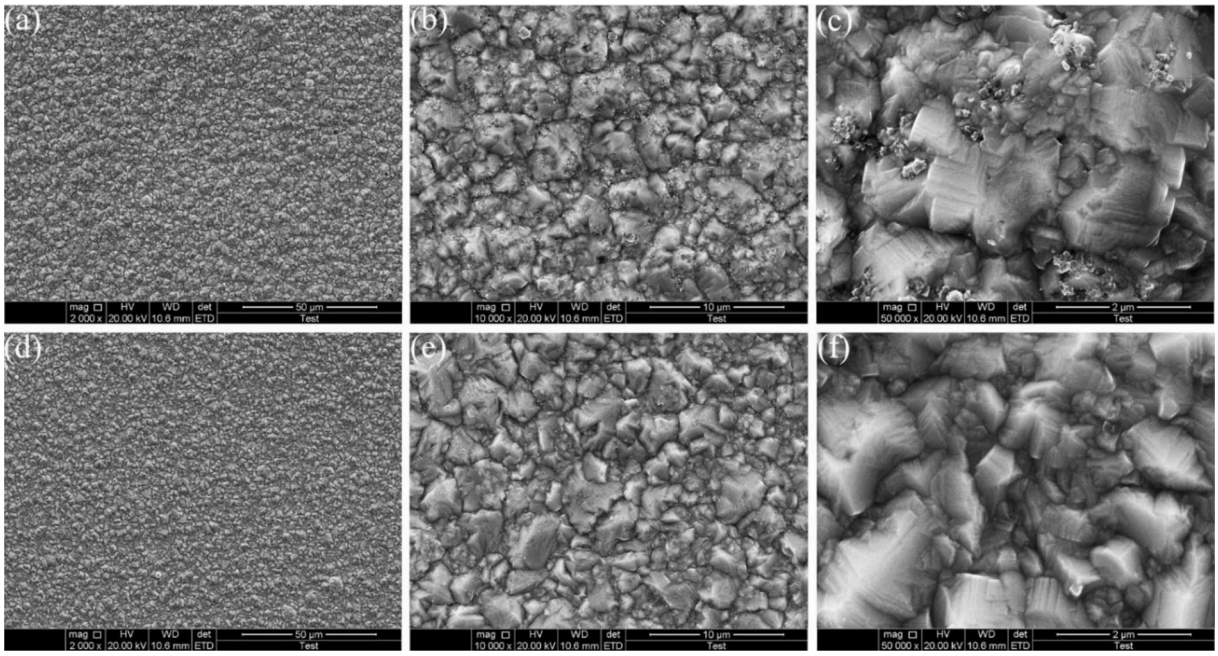

Fig. 5. SEM micrographs of the Ni/diamond composite coating electrodeposited under (a-c) magnetic stirring and (d-f) ultrasonic agitation.

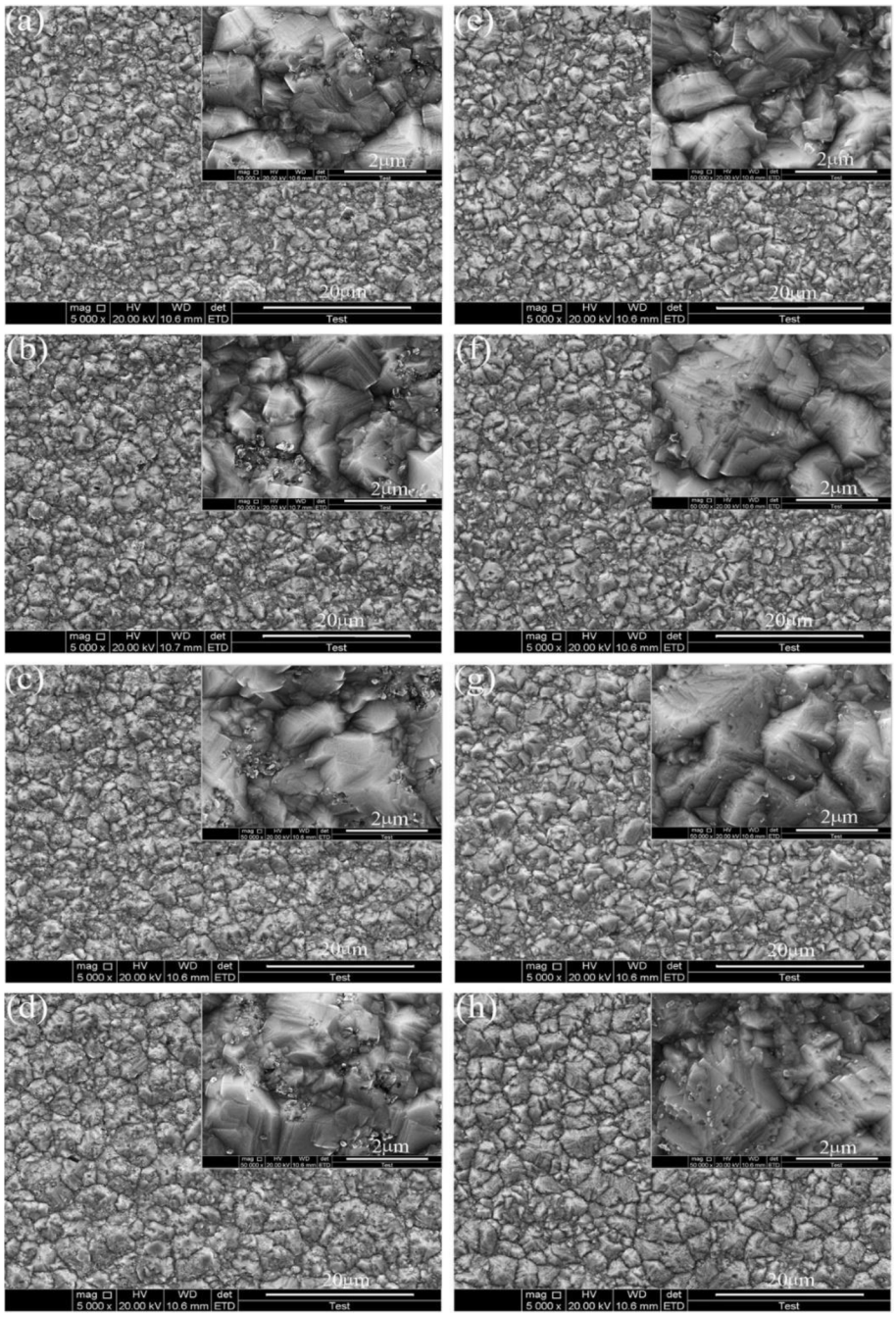

Fig. 6. SEM micrographs of the Ni/diamond composite coatings electrodeposited under (a-d) magnetic stirring, (e-h) ultrasonic agitation at (a, e) 2 A dm^{-2}, (b, f) 3 A dm^{-2}, (c, g) 4 A dm^{-2} and (d, h) 5 A dm^{-2}.

prepared under ultrasonic agitation contained 9.2–11.4 wt% diamond particles. Increasing current density from 2 to 5 A dm^{-2}, the embedded diamond content first increases to 11.4 wt% at 3 A dm^{-2}, beyond which it steadily decreases to 9.9 wt% at 5 A dm^{-2}. Compared to mechanical stirring, the agglomeration of the nanoparticles under ultrasonic agitations are few. So, the ultrasonic-assisted electrodeposited Ni/diamond composite coatings have few adsorbed and aggregated particles on the surface. Therefore, the amounts of the co-deposited diamond for ultrasonic-assisted electrodeposited Ni/diamond coating are slightly lower than the magnetic mode. However, the dispersion state of the diamond particles in the ultrasonic-assisted electrodeposits are better, which benefits the coating performance.

3.3. Phase structure and crystallite size

Fig. 8 displays the XRD patterns of the ultrasonic-assisted electrodeposited samples at different current density. As seen in Fig. 8, the spectra show two diffraction peaks, corresponding to the 2θ at 44.5° and 51.8°. The peaks at 44.5° and 51.8° belong to Ni (1 1 1) and Ni (2 0 0) crystal planes. It was observed that as current density increased from 2 to 5 A dm^{-2}, the peak intensity of (1 1 1) texture gradually decreased, but the peak intensity of the (2 0 0) plane steadily increased. The sharp and narrow diffraction peaks indicate the crystallographic texture of the coatings. The peak of the diamond at 43.9° were not noticed, due to the low content in the matrix. Table 3 presents the RTC and crystallite size of the obtained coating under ultrasonic agitation. It demonstrated that the preferred orientation was (2 0 0) textures. As current density increases,

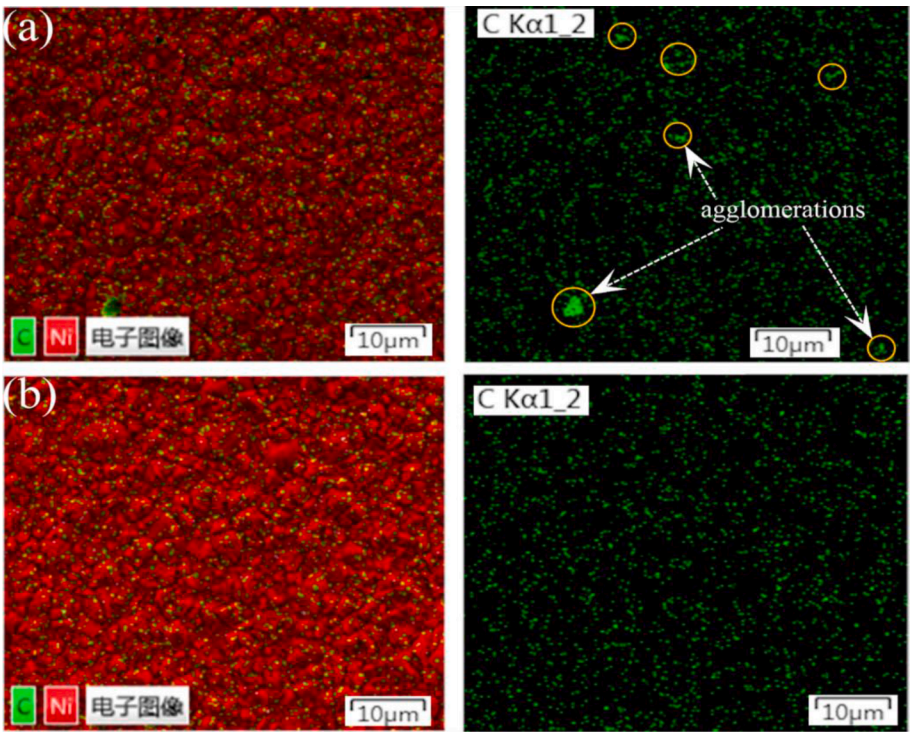

Fig. 7. Element distribution maps of the Ni/diamond coating electrodeposited under (a) magnetic stirring and (b) ultrasonic agitation.

Table 2
Chemical composition of the Ni/diamond coatings deposited under ultrasonic agitation.

Element (wt. %)	Sample, 2 A dm^{-2}	Sample, 3 A dm^{-2}	Sample, 4 A dm^{-2}	Sample, 5 A dm^{-2}
Ni	90.8	88.6	89.5	90.1
C/diamond	9.2	11.4	10.5	9.9

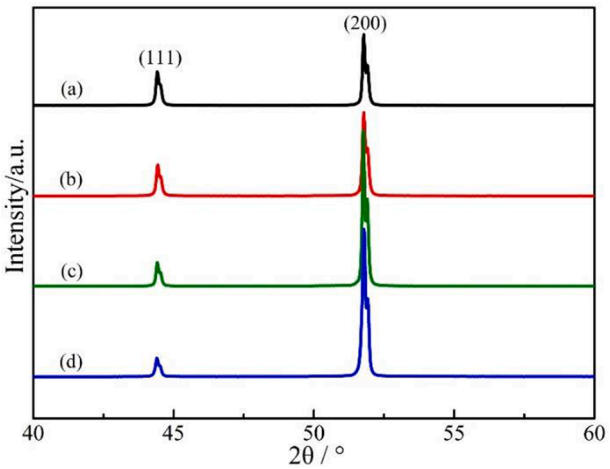

Fig. 8. XRD spectra of Ni/diamond composite coating electrodeposited under ultrasonic agitation. at current density (a) 2 A dm^{-2}, (b) 3 A dm^{-2}, (c) 4 A dm^{-2} and (d) 5 A dm^{-2}.

the RTC value of the (200) plane increases from 76.3% up to 93.4%. In contrast, the RTC value of the (111) plane reduces from 22.8% down to 5.7%. The crystallite size of the sample coatings calculated on the (200) plane was summarized in Table 3. It manifests that the crystallite size was about 60–80 nm and the finest grains size of 59 nm was obtained at

Table 3
RTC and crystallite size of the Ni/diamond composite coatings.

Samples	RTC / %			Crystallite size (nm)		
	(111)	(200)	(220)	(111)	(200)	(220)
2 Adm^{-2}	22.8	76.3	0.9	50	76	43
3 Adm^{-2}	16.4	82.0	1.6	51	67	26
4 Adm^{-2}	8.5	90.8	0.7	54	82	33
5 Adm^{-2}	5.7	93.4	0.9	50	59	30

5 A dm^{-2}. The optimal current density was increased for ultrasonic-assisted electrodeposition. Current density could influence the microstructure of the Ni/diamond composites.

3.4. Surface topography and roughness

Fig. 9. displays the surface topography of Ni/diamond coatings. It was evident that the sample coating electrodeposited under magnetic agitation presents hill-valley like topography. It comprises granular protrusions in size of 1–3 μm and interlaced gullies (Fig. 9a, b). The protrusions are the clusters of the Ni crystals. When ultrasonic agitation was employed during the electrodeposition process, the surface of Ni/diamond coating (Fig. 9c, d) seems smoother. Compared to Fig. 9a, Fig. 9c indicated that the growth orientation of Ni crystal lattices was significantly consistent under the influence of ultrasound. The coating prepared by ultrasonic-assisted electrodeposition has a certain growth orientation. This is due to that the ultrasonic assistance decreased the stress of (200) texture in the Ni/diamond composite coating. So, the nickel grains are easy to grow along the (200) crystal plane. This phenomenon was consistent with the XRD results. As Table 3 shows, the ultrasonic-assisted coating has high RTC values of (200) plane which was in the range of 76–94%. The 2D images (Fig. 9b, d) indicate that the ultrasonic-assisted deposited sample is more compact and has fewer particle aggregations. No microcracks or pinpores have been observed, revealing the dense coatings. The analysis by Nanoscope Analysis Software showed that the ultrasound-assisted Ni/diamond coating owns fine structure in comparison with magnetic mode. The average roughness

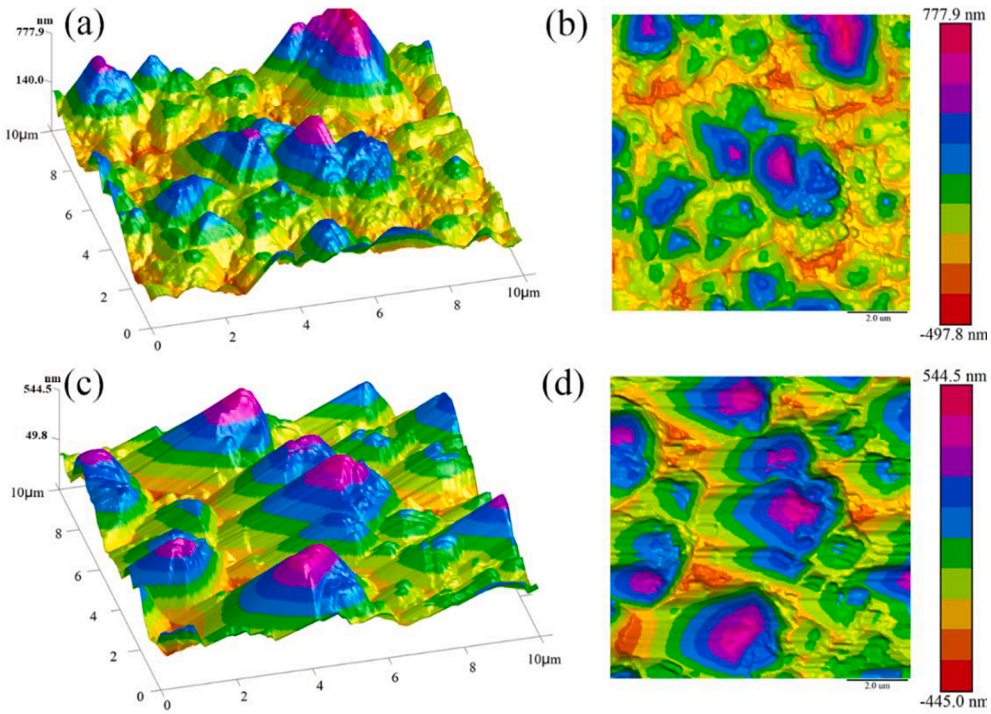

Fig. 9. Surface topography of the Ni/diamond coating electrodeposited under (a, b) magnetic stirring and (c, d) ultrasonic agitation.

(R_a) and root mean square roughness (R_q) of the two coatings are listed in Table 4. The R_a of the samples prepared under magnetic and ultrasonic agitations were 116 nm, 110 nm, respectively. So, the ultrasonic-assisted electrodeposited coating is smoother. Compare Table 4 with Fig. 4, it might be felt that the roughness data and the surface photos are not consistent. It is well known that the same sample could show different morphological characteristics at different scales, such as cm, μm and nm scale. It might be the result of a combination of two opposing factors that affect the final morphologies of the coatings. On the one hand, ultrasonic assistance is beneficial to the full dispersion of the nanoparticles, leading to the uniform distribution of the particles and the even surface. On the other hand, the amounts of the embedded particles increased much with the assistance of ultrasonic waves, which can increase the protrusion structure of the obtained coatings.

3.5. Electrochemical co-deposition mechanism

Fig. 10 displays the mechanism of electrochemical co-deposition for Ni/diamond coatings. As for Fig. 10(a), the nanoparticles were positively charged by absorbing Ni^{2+} metallic ions on the surface. When powering off and without stirring, a lot of particle aggregations suspend in the electrolyte. When power on and magnetic stirring, as shown in Fig. 10(b), partial particle aggregations are dispersed. Affected by the electric field and magnetic stirring, the Ni^{2+} ions and the charged particles transported to and adsorbed on the cathodic surface. Then, Ni^{2+} ions acquired electrons and were reduced to Ni atoms. Finally, the nanodiamonds were strongly wrapped by nickel crystals and the Ni/diamond composite coatings have been formed. However, under magnetic stirring condition, the aggregations have not been well dispersed in the solution, leading to some aggregates in the deposits, which will decrease the coating performance. As for the ultrasonic-assisted electrodeposition, the ultrasonic waves could form cavitation in high-frequency oscillation, which can fully disperse nanoparticles, as presented in Fig. 10(c). Tiny bubbles grow up quickly, and burst, resulting in the formation of cavitation jets which would promote the dispersion of the aggregated diamond particles. As a result, a more uniform distribution of the co-deposited particles has been achieved.

Table 4
The R_a and R_q of the Ni/diamond composite coatings.

Coating samples	R_a, nm	R_q, nm
Magnetic agitation	116	146
Ultrasonic agitation	110	138

3.6. Element chemical states of the coating surface

Fig. 11 displays the XPS spectra of the Ni/diamond coating surface. As shown in Fig. 11(a), Ni, O and C elements have been detected in the XPS survey spectrum. The C1s can be ascribed to the dispersed nanodiamonds in the composite coatings. The Ni2p XPS spectra were presented in Fig. 11 (b). $Ni2p_{3/2}$ XPS have three split peaks, belonging to metallic Ni, nickel oxides or hydroxides, and satellites nickel, respectively. Generally, exposure to air, nickel coating surface would produce an oxide film. However, in comparison with the Ni-B[34,35], Ni-Co [36,37] matrix composite coating, the oxidation degree of the Ni/diamond coating surface is lower and the content of metallic nickel is higher. Meanwhile, due to the hydrogen evolution reaction at the cathode, OH^- ions have been generated, then nickel hydroxides were formed [38]. Fig. 11 (c) depicts the C1s XPS spectra and four fitted peaks were observed. As indicated in Fig. 11(c), from 284.3 to 288.5 eV, the four peaks were ascribed to C–H, C–C, C-O, COO– species, respectively. The C–C peaks reflect the existence of nanodiamonds in the electrodeposits. O1s XPS spectrum was given in Fig. 11. (d). The peaks at 529.4 eV, 530.9 eV, 531.5 eV and 532.4 eV belong to Ni-O, O^{2-}, OH^- and H_2O species, respectively.

3.7. Electrochemical characteristics

Fig. 12 displays the EIS curves of the Ni/diamond composite coatings electrodeposited at 2, 3, 4 and 5 A dm^{-2} under ultrasonic agitation after immersed 0.5 h in 3.5 wt% NaCl aqueous solution. The adopted equivalent electrical circuit (EEC) models were given in Fig. 13. Here, R_s is solution resistance. CPE_{dl} reflects the double-layer capacitance. R_{ct} is the

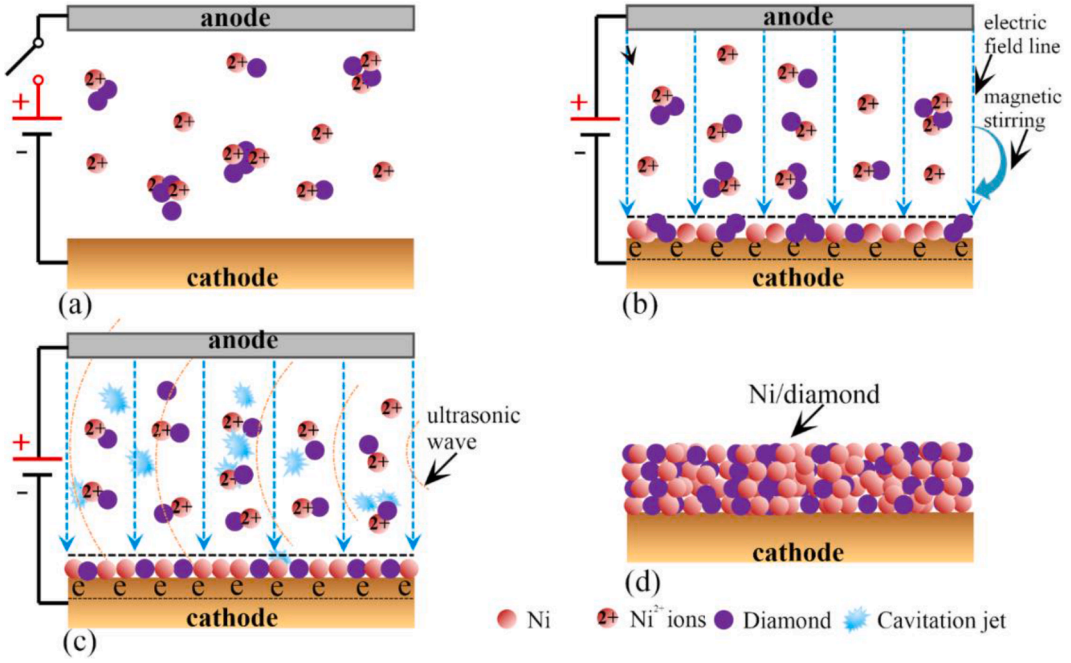

Fig. 10. Schematic of electrochemical co-deposition mechanism of Ni/diamond coatings (a) power off, (b) magnetic stirring, (c) ultrasonic agitation and (d) the obtained coatings.

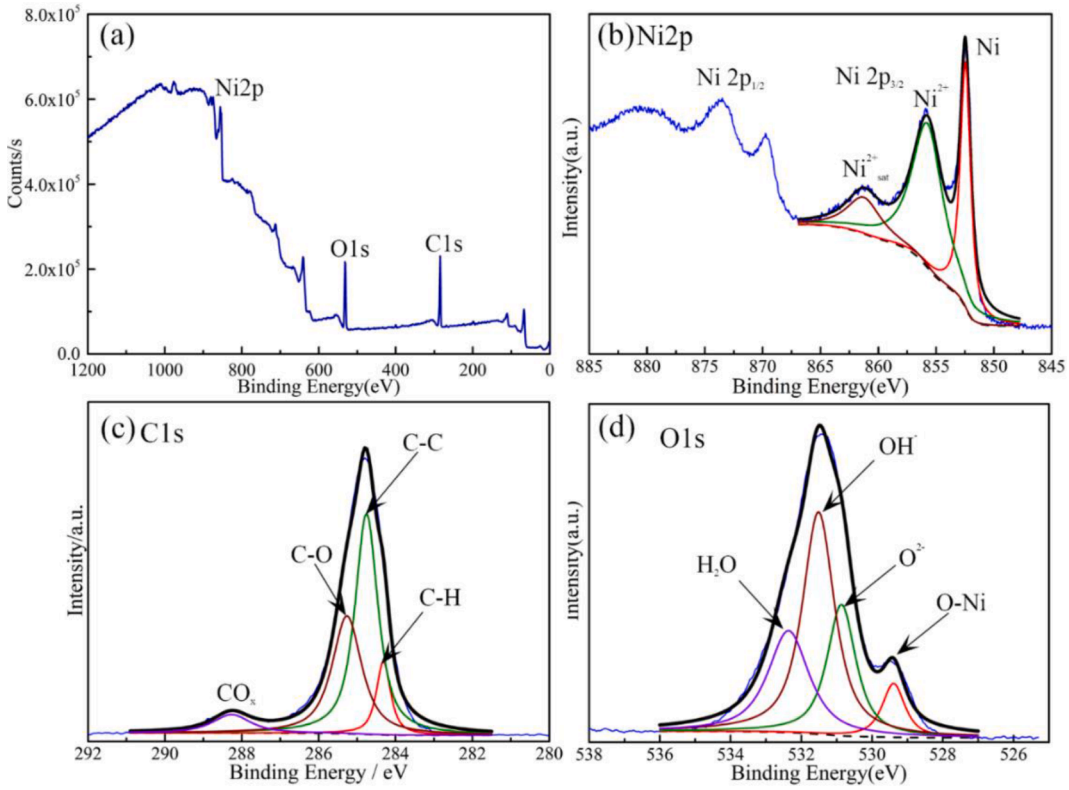

Fig. 11. XPS patterns of (a) survey, (b) Ni 2p, (c) C 1 s and (d) O1s of Ni/diamond composite coating.

charge transfer resistance. CPE_c and R_c are coating capacitance and coating resistance, respectively. When soaked for 30 min, the two-time constant EEC model Fig. 13(b) was selected to fit the EIS data. Table 5 listed the corrosion parameters. As observed in Table 5, the R_p ($\approx R_c + R_{ct}$) value of the samples first increases as current density increases, then decreases when beyond 4 A dm^{-2}. The maximum R_p of 39.9 kΩ cm^2 was obtained at 4 A dm^{-2}, signifying the best corrosion resistance.

When immersed 7 days (about 168 h), as can be seen in Fig. 14, all the Nyquist curves still exhibited semi-ellipse shape with different radius. This indicated that the corrosion mechanism has not changed and the one-time constant EEC model of Fig. 13(a) was used to fit the EIS curves. The fitted data of the EIS curves were given in Table 6. It shows

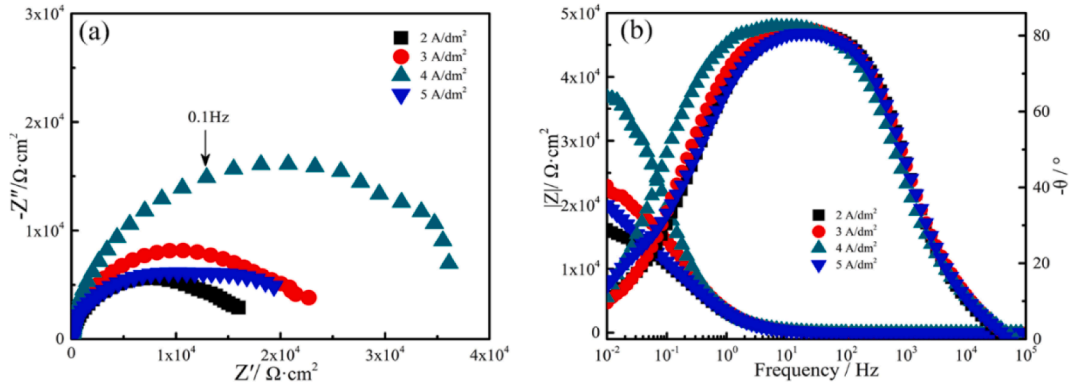

Fig. 12. Nyquist and bode curves of Ni/diamond coatings electrodeposited under ultrasonic agitation after immersed 30 min.

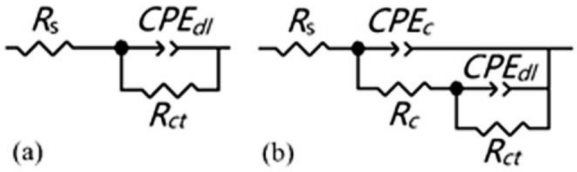

Fig. 13. Equivalent electrical circuit (EEC) models.

that the sample of 4 A dm^{-2} has the maximum R_{ct} of 50.3 kΩ cm^2, illustrating the best corrosion resistance. It indicated that 4 A dm^{-2} was a suitable parameter for the ultrasonic-assisted electrodeposited Ni/diamond with good corrosion resistance.Table 7.

Fig. 15 presents the Tafel plots of Ni/diamond coating deposited at different current density after immersed 14 days. As can be seen, the corrosion resistance of the samples has changed after immersed for 14 days. In this case, the samples of 4 A dm^{-2} still has the maximum R_p of 43.33 kΩ·cm^2, indicating excellent corrosion resistance. However, the E_{corr} was slightly negative and the i_{corr} was slightly larger than the sample of 5 A dm^{-2}. This is because a series of changes occurred on the surface structure and corrosion mechanism with the soaking time. Ultrasonic agitation and 4 A dm^{-2} are helpful to the enhancement of the

Table 6
Corrosion parameters for Ni/diamond coating prepared under ultrasonic agitation when immersed 168 h.

Ni/diamond	R_s (Ω·cm^2)	R_{ct}(kΩ·cm^2)	CPE_{dl}(μF cm^{-2})	n
2 A dm^{-2}	3.5	44.5	53.0	0.93
3 A dm^{-2}	3.7	34.7	52.2	0.91
4 A dm^{-2}	3.5	50.3	54.3	0.93
5 A dm^{-2}	4.6	30.7	54.8	0.92

Table 7
Corrosion parameters of Ni/diamond coating after immersed 14 days.

Ni/diamond	E_{corr} (V vs.SCE)	i_{corr}/μA·cm^{-2}	R_p/kΩ·cm^2
2 A/dm^2	−0.31	0.66	41.07
3 A/dm^2	−0.32	0.74	36.25
4 A/dm^2	−0.31	0.67	43.33
5 A/dm^2	−0.29	0.62	41.18

Table 5
Corrosion parameters for Ni/Diamond composite coating when immersed 30 min.

Ni/Diamond	R_s(Ω·cm^2)	R_c(kΩ·cm^2)	CPE_c(μF cm^{-2})	n_1	R_{ct}(kΩ·cm^2)	CPE_{dl}(μF cm^{-2})	n_2
2 A dm^{-2}	4.4	9.6	52.7	0.93	9.1	238.6	0.58
3 A dm^{-2}	4.7	16.7	50.1	0.92	10.0	419.4	0.78
4 A dm^{-2}	5.1	33.9	56.3	0.92	6.0	756.2	0.96
5 A dm^{-2}	4.6	10.5	52.2	0.92	13.3	267.0	0.69

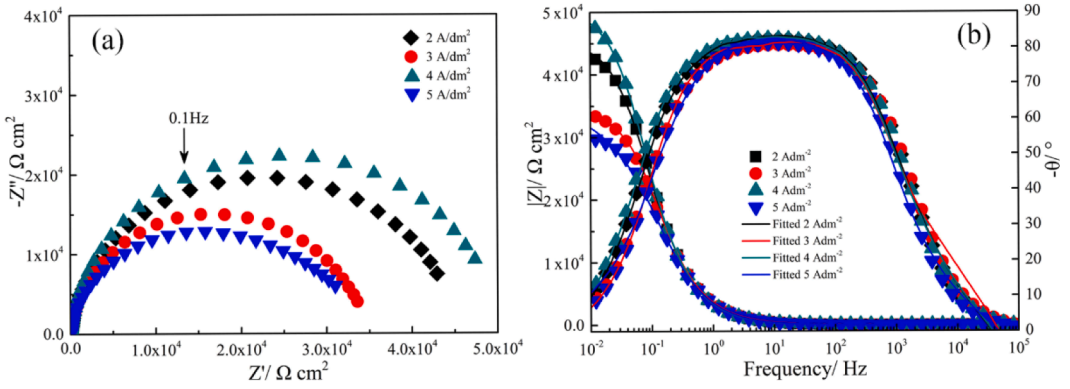

Fig. 14. Nyquist and bode curves of Ni/diamond coatings electrodeposited under ultrasonic agitation after immersed 168 h.

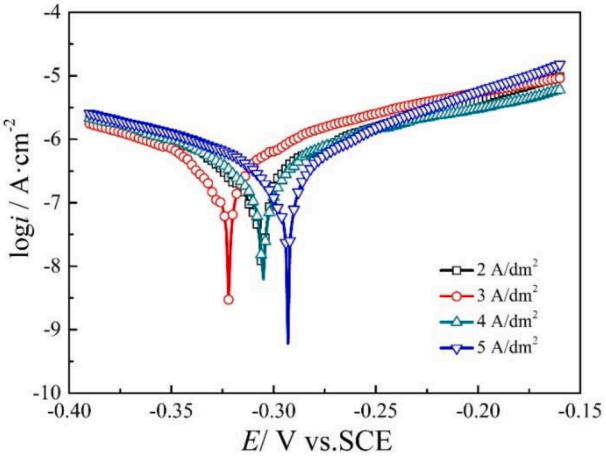

Fig. 15. Tafel curves of Ni/diamond coating after immersed 14 days.

anti-corrosion capability of the Ni/diamond coatings.

4. Conclusions

This work has investigated the ultrasonic-assisted electrodeposition of Ni/diamond composite coatings and their structure and electrochemical properties. The influence of ultrasonic agitation and current density on the composition, morphology, surface topography, phase structure, and corrosion resistance were evaluated. These Ni/diamond coatings own dense and granular like morphology with pyramid-like grains. The deposits contain 9.2–11.4 wt% diamond particles, which were uniformly distributed in the coating. With the increase of current density, the amounts of diamond in ultrasonic-assisted electrodeposits first increased and then decreased with a maximum of 11.4 wt% at 3 A dm^{-2}. Meanwhile, the RTC of the preferred orientation (200) plane of the Ni/diamond coating increases from 76.3% up to 93.4%. The growth orientation of the ultrasonic-assisted deposited Ni crystal lattices is more consistent. The average roughness (R_a) of the ultrasonic-assisted coatings was 110 nm, which was lower than that of 116 nm for magnetic stirrings. The maximum R_p of 39.9, 50.3 kΩ cm^2 was obtained at 4 A dm^{-2} when respectively immersed 30 min and 7 days, indicating the best corrosion resistance of the coatings of 4 A dm^{-2}. A more uniform distribution of the co-deposited particles has been achieved with ultrasonic assistance. Ultrasonic agitation and 4 A dm^{-2} is helpful to increase the corrosion-resistant capability of the Ni/diamond coatings.

Declaration of Competing Interest

The authors declare that they have no known competing financial interests or personal relationships that could have appeared to influence the work reported in this paper.

Acknowledgments

We would like to thank the National Natural Science Foundation of China (Grant No. 51679076, 52079048), Jiangsu Provincial Key Research and Development Program (BE2020780) for their financial support.

References

[1] M.S. Safavi, A. Rasooli, Ni-P-TiO_2 nanocomposite coatings with uniformly dispersed Ni_3Ti intermetallics: Effects of current density and post heat treatment, Surf. Coat. Technol. 372 (2019) 252–259.
[2] H. Li, M. Kang, Y. Zhang, Y. Liu, M. Jin, N. Mbugua, G. Zhu, C. Liu, Fabrication of Ni–Co–BN (h) Nanocomposite Coatings with Jet Electrodeposition in Different Pulse Parameters, Coatings 9 (2019) 50.
[3] K. Akhtar, U. Hira, H. Khalid, N. Zubair, Uniform fine particles of ZrO_2 as reinforcement filler in the electrodeposited Cu-ZrO_2 nanocomposite coating on steel substrate, J. Alloys Compd. 772 (2019) 15–24.
[4] B. Li, D. Li, J. Zhang, W. Chen, W. Zhang, Electrodeposition of Ni-W/TiN-Y_2O_3 nanocrystalline coating and investigation of its surface properties and corrosion resistance, J. Alloys Compd. 787 (2019) 952–962.
[5] Z. Mahidashti, M. Aliofkhazraei, N. Lotfi, Review of Nickel-Based Electrodeposited Tribo-Coatings, Transactions of the Indian Institute of Metals 71 (2017) 257–295.
[6] A. Karimzadeh, M. Aliofkhazraei, F.C. Walsh, A review of electrodeposited Ni-Co alloy and composite coatings: Microstructure, properties and applications, Surf. Coat. Technol. 372 (2019) 463–498.
[7] W. Jiang, L. Shen, M. Xu, Z. Wang, Z. Tian, Mechanical properties and corrosion resistance of Ni-Co-SiC composite coatings by magnetic field-induced jet electrodeposition, J. Alloys Compd. 791 (2019) 847–855.
[8] P. Jin, C. Sun, C. Zhou, L. Shi, C. Liu, Effect of SiC particle size on structures and properties of Ni–SiC nanocomposites deposited by magnetic pulse electrodeposition technology, Ceram. Int. 45 (2019) 20155–20164.
[9] Z. Geng, Y. Liu, H. Zhang, Tribological properties of electrodeposited Ni–ZrO_2 nanocomposite coatings on copperplate of crystallizer, Surf. Eng. 35 (2018) 919–926.
[10] Y. Li, S. Geng, G. Chen, Electrodeposited Ni/CeO_2 mulriple coating on SUS 430 steel interconnect, Int. J. Hydrogen Energy 43 (28) (2018) 12811–12816.
[11] H. Majidi, M. Aliofkhazraei, A. Karimzadeh, A.S. Rouhaghdam, Corrosion and wear behaviour of multilayer pulse electrodeposited Ni–Al_2O_3 nanocomposite coatings assisted with ultrasound, Bull. Mater. Sci. 39 (2016) 1691–1699.
[12] K. Hou, T. Han, H. Sheu, M. Ger, Preparation and wear resistance of electrodeposited Ni–W/diamond composite coatings, Appl. Surf. Sci. 308 (2014) 372–379.
[13] H. Zhou, N. Du, J. Guo, S. Liu, A new insight into promotion action of Co^{2+} in Ni-diamond composite electrodeposition, Journal of Materials Science & Technology 35 (2019) 1797–1802.
[14] H. Mazaheri, S.R. Allahkaram, Deposition, characterization and electrochemical evaluation of Ni–P–nano diamond composite coatings, Appl. Surf. Sci. 258 (2012) 4574–4580.
[15] J. Deng, J. Zhang, Y. Tu, P. Yang, M. An, P. Wang, Effect of BEO in the electrodeposition process of Ni/diamond composite coatings for preparation of ultra-thin dicing blades: Experiments and theoretical calculations, Ceram. Int. 44 (14) (2018) 16828–16836.
[16] M. Sajjadnejad, H. Omidvar, M. Javanbakht, A. Mozafari, Textural and structural evolution of pulse electrodeposited Ni/diamond nanocomposite coatings, J. Alloys Compd. 704 (2017) 809–817.
[17] H. Bao, Q. Li, H. Jia, G. Yang, Mechanical properties comparison of Ni-diamond composite coatings fabricated by different methods, Materials Research Express 6 (2019), 106425.
[18] W. Huang, Y. Zhao, X. Wang, Preparing a high-particle-content Ni/diamond composite coating with strong abrasive ability, Surf. Coat. Technol. 235 (2013) 489–494.
[19] I. Makarova, I. Dobryden, D. Kharitonov, A. Kasach, J. Ryl, E. Repo, E. Vuorinen, Nickel-nanodiamond coatings electrodeposited from tartrate electrolyte at ambient temperature, Surf. Coat. Technol. 380 (2019), 125063.
[20] S. Sahay, M.K. Pandey, A.K. Kar, Metal concentration dependent mechanical properties of electrodeposited nickel incorporated diamond like carbon (Ni-DLC) thin films studied by nanoindentation, Appl. Surf. Sci. 489 (2019) 73–79.
[21] L. Xiang, Q. Shen, Y. Zhang, W. Bai, C. Nie, One-step electrodeposited Ni-graphene composite coating with excellent tribological properties, Surf. Coat. Technol. 373 (2019) 38–46.
[22] C.Y. Ma, D.Q. Zhao, F.F. Xia, H. Xia, T. Williams, H.Y. Xing, Ultrasonic-assisted electrodeposition of Ni-Al_2O_3 nanocomposites at various ultrasonic powers, Ceram. Int. 46 (2020) 6115–6123.
[23] W. Cui, Y. Zhang, R. Song, P. Wang, Ultrasonic assisted pulse electrodeposited Ni-doped TiN coatings, Ceram. Int. 44 (2018) 14767–14773.
[24] I. Tudela, Y. Zhang, M. Pal, I. Kerr, T.J. Mason, A.J. Cobley, Ultrasound-assisted electrodeposition of nickel: Effect of ultrasonic power on the characteristics of thin coatings, Surf. Coat. Technol. 264 (2015) 49–59.
[25] J.M. Costa, A.F.d. Almeida Neto, Ultrasound-assisted electrodeposition and synthesis of alloys and composite materials: A review, Ultrason Sonochem 68 (2020) 105193, https://doi.org/10.1016/j.ultsonch.2020.105193.
[26] H. Zhang, N. Zhang, F. Fang, Fabrication of high-performance nickel/graphene oxide composite coatings using ultrasonic-assisted electrodeposition, Ultrason Sonochem 62 (2020), 104858.
[27] M. Ridošić, E. García-Lecina, A. Salicio-Paz, J. Bajat, The advantage of ultrasound during electrodeposition on morphology and corrosion stability of Zn-Co alloy coatings, Transactions of the IMF 98 (2020) 114–120.
[28] E.J. Ekoi, D.P. Dowling, Evaluation of the microstructure, mechanical and tribological properties of nickel-diamond nanocomposite coatings, Diamond Relat. Mater. 94 (2019) 118–128.
[29] M. Sajjadnejad, H. Omidvar, M. Javanbakht, Influence of Pulse Operational Parameters on Electrodeposition, Morphology and Microstructure of Ni/nanodiamond Composite Coatings, Int. J. Electrochem. Sci. 12 (2017) 3635–3651.
[30] P.A. Orrillo, S.B. Ribotta, L.M. Gassa, G. Benítez, R.C. Salvarezza, M.E. Vela, Phosphonic acid functionalization of nanostructured Ni–W coatings on steel, Appl. Surf. Sci. 433 (2018) 292–299.
[31] B. Li, W. Zhang, D. Li, Y. Huan, J. Dong, Microstructural, surface and electrochemical properties of a novel Ni–B/Ni–W–BN duplex composite coating by co-electrodeposition, Appl. Surf. Sci. 458 (2018) 305–318.

[32] A. Rasooli, M.S. Safavi, M. Kasbkar Hokmabad, Cr_2O_3 nanoparticles: A promising candidate to improve the mechanical properties and corrosion resistance of Ni-Co alloy coatings, Ceram. Int. 44 (2018) 6466–6473.
[33] B. Bakhit, A. Akbari, F. Nasirpouri, M.G. Hosseini, Corrosion resistance of Ni–Co alloy and Ni–Co/SiC nanocomposite coatings electrodeposited by sediment codeposition technique, Appl. Surf. Sci. 307 (2014) 351–359.
[34] M. Salari Mehr, A. Akbari, E. Damerchi, Electrodeposited Ni-B/SiC micro- and nano-composite coatings: A comparative study, J. Alloys Compd. 782 (2019) 477–487.
[35] D. Zhang, X. Cui, G. Jin, Z. Cai, M. Dong, Thermal stability of Ni-B/La_2O_3 coatings by electro-brush plating technique, Surf. Coat. Technol. 349 (2018) 1042–1047.
[36] P.R. Dheeraj, A. Patra, S. Sengupta, S. Das, K. Das, Synergistic effect of peak current density and nature of surfactant on microstructure, mechanical and electrochemical properties of pulsed electrodeposited Ni-Co-SiC nanocomposites, J. Alloys Compd. 729 (2017) 1093–1107.
[37] B. Bakhit, The influence of electrolyte composition on the properties of Ni-Co alloy coatings reinforced by SiC nano-particles, Surf. Coat. Technol. 275 (2015) 324–331.
[38] B. Li, W. Zhang, T. Mei, Y. Miao, Fabrication of Ni–B/TiC–Y_2O_3 nanocomposites by one-step electrodeposition at different duty cycle and evaluation of structural, surface and performance as protective coating, J. Alloys Compd. 823 (2020), 153888.